Nanoscale

PAPER

View Article Online
View Journal | View Issue

Cite this: *Nanoscale*, 2015, **7**, 16789

A self-amplified transistor immunosensor under dual gate operation: highly sensitive detection of hepatitis B surface antigen†

I.-K. Lee,‡[a,b] M. Jeun,‡[a] H.-J. Jang,[b] W.-J. Cho[b] and K. H. Lee*[a]

Received 13th May 2015,
Accepted 29th August 2015

DOI: 10.1039/c5nr03146j

www.rsc.org/nanoscale

Ion-sensitive field-effect transistors (ISFETs), although they have attracted considerable attention as effective immunosensors, have still not been adopted for practical applications owing to several problems: (1) the poor sensitivity caused by the short Debye screening length in media with high ion concentration, (2) time-consuming preconditioning processes for achieving the highly-diluted media, and (3) the low durability caused by undesirable ions such as sodium chloride in the media. Here, we propose a highly sensitive immunosensor based on a self-amplified transistor under dual gate operation (immuno-DG ISFET) for the detection of hepatitis B surface antigen. To address the challenges in current ISFET-based immunosensors, we have enhanced the sensitivity of an immunosensor by precisely tailoring the nano-structure of the transistor. In the pH sensing test, the immuno-DG ISFET showed superior sensitivity (2085.53 mV per pH) to both standard ISFET under single gate operation (58.88 mV per pH) and DG ISFET with a non-tailored transistor (381.14 mV per pH). Moreover, concerning the detection of hepatitis B surface antigens (HBsAg) using the immuno-DG ISFET, we have successfully detected trace amounts of HBsAg (22.5 fg mL^{-1}) in a non-diluted 1× PBS medium with a high sensitivity of 690 mV. Our results demonstrate that the proposed immuno-DG ISFET can be a biosensor platform for practical use in the diagnosis of various diseases.

1. Introduction

Hepatitis B virus (HBV) is an infectious virus that causes several hepatic diseases such as hepatitis B, hepatic insufficiency, liver cirrhosis, and liver cancer.[1,2] Currently, about 2 billion people worldwide are infected with HBV, and of that number, 350 million people have developed chronic hepatitis B (CHB).[3–5] CHB is generally known to be the more lethal disease compared to other hepatitis types because most people with CHB tend to be asymptomatic and are unaware that they have it.[6]

Once a person has developed CHB, the incidence rates of cirrhosis and liver cancer increase with time, and the infectees are unwilling sources of infection and can transmit their own virus to other people. Therefore, a regular medical check-up is necessary. Serodiagnoses that include an enzyme-linked immunosorbent assay (ELISA) and a radioimmuno assay (RIA) have been widely used in clinics for HBV diagnosis.[7,8] In these medical tests, HBV is detected by confirming the chemiluminescence emitted by an antigen–antibody reaction. However, these diagnostic processes are barely suitable for regular medical check-ups because they take a long time and are expensive. In addition, the serodiagnoses lack the sensitivity and specificity needed to obtain more precise test results.

An ion-sensitive field-effect transistor (ISFET) is an electrochemical sensor[9–11] which can sensitively detect a signal resulting from the interaction of an analyte with a biological element, and can accurately transform the signal into an electrical signal. So far, ISFETs based on carbon nanotubes (CNTs), graphene, or nanowires (NWs) have received considerable attention as potential diagnosis devices (or biosensors) for easy and fast regular medical check-ups[12–21] because they possess several desirable characteristics such as fast detection time, low manufacturing cost, high reliability, the possibility of label-free and multiplexing detection, and portability.[22] However, their clinical applications have been limited to pH sensors owing to the following critical problem. Standard ISFETs are driven by a single gate (SG) operation mode and

[a]*Center for Biomaterials, Biomedical Research Institute, Korea Institute of Science and Technology (KIST), 5 Hwarang-ro 14-gil, Seongbuk-gu, Seoul 136-791, Republic of Korea. E-mail: kwanhyi@kist.re.kr*

[b]*Department of Electronic Materials Engineering, Kwangwoon University, 20 Gwangun-ro, Nowon-gu, Seoul 139-701, Republic of Korea*

†Electronic supplementary information (ESI) available: Material preparation, surface functionalization and anti-HBsAg immobilization. See DOI: 10.1039/c5nr03146j

‡These authors have contributed equally to this work.

their sensitivities are only determined by a change in the surface potential of the sensing membrane.[23] Thus, despite many efforts to enhance the sensitivity, standard ISFETs still have very poor sensitivity because the changes in the surface potential caused by biological events such as protein interactions and DNA hybridization are quite small.

As a solution to this problem, a dual gate ISFET (DG ISFET) was proposed.[24,25] A DG ISFET significantly amplifies the small changes in the surface potential without additional amplification circuits by inducing a capacitive coupling between the top and bottom gate dielectrics in the transistor.[26–28] However, its applications have still not been used as a biosensor for practical applications, because of another problem, the Debye screening length issue.[25,29]

The sensing performance of an ISFET is severely affected by the Debye screening length (λ_D), which is a particular distance where the charges on the analyte are electrically screened by the ions in media;[30] the λ_D is completely dependent on the ionic strength (or ion concentration) of the media such as physiological solutions or phosphate buffered saline (PBS).[31] The λ_D decreases as the ionic strength increases and a short λ_D results in a lower sensitivity of the ISFET because the ISFET cannot detect chemical interactions beyond the λ_D in the media.[22] In the case of body fluids (blood, serum, urine) and undiluted PBS buffer solutions (1× PBS), the λ_D is very short because they have high ion concentration (generally higher than 100 mM). Therefore, to overcome the poor sensitivity caused by the short λ_D issue, fussy preconditioning processes such as centrifugation, filtration, and dilution of the media are necessarily required.[32] However, these time-consuming steps do not meet the needs of the ISFET for on-the-site practical applications.

In this study, we first used the DG ISFET as an immunosensor for detecting the hepatitis B surface antigen (HBsAg). In order to avoid the time-consuming steps and to effectively detect the HBsAg in undiluted 1× PBS, we dramatically enhanced the sensitivity of the DG ISFET by delicately tailoring the nanostructure of the transistor, which directly influences the amplification factor of sensitivity in the DG ISFET. Our research demonstrates that the tailored DG ISFET immunosensor (immuno-DG ISFET) can help us to address the challenges in current transistor-based immunosensors: the poor sensitivity caused by short λ_D in media with high ion concentration, time-consuming preconditioning processes for obtaining the highly-diluted media, and the low sensor durability caused by undesirable ions such as sodium chloride in the media.

2. Experimental

2.1. Fabrication of ISFET

The structure of the ISFET is basically the same as the structure of a metal–oxide semiconductor field-effect transistor (MOSFET), but parts of the metal gate electrode and the gate dielectric in the MOSFET are replaced by sensing components composed of a reference electrode, a chamber, an electrolyte solution, and a sensing membrane. Thus, the ISFET comprises a FET part (transducer) and a sensing part. In this work, we separated the sensing portion of the ISFET to protect the transducer from the ion damage resulting from undesirable ions such as sodium chloride in solution. The separated sensing component is aptly named the 'extended-gate (EG) sensing device'. The ISFET with the EG sensing device offers high durability regarding the sensing performance of the sensor and is well positioned to be commercialized because it has not only a reusable transducer, but also a deposable EG sensing device.

2.1.1. Fabrication of the transistor (transducer part). To fabricate the transistors to use in the DG operation, a p-type (100) silicon-on-insulator (SOI) wafer with a 200 nm-thick buried oxide (BOX) layer as a bottom gate oxide was used as the starting material. The thickness of the top silicon layer (resistivity: 10 Ω cm, doping level: 1×10^{15} cm^{-3}) of the SOI wafer was 100 nm and it was etched to a thickness of 20 nm using a 2.38% tetramethyl ammonium hydroxide (TMAH) solution for precise thickness control.

After a standard cleaning process, the active region was formed using photolithography and a reactive ion etching (RIE) process. Then, a phosphorus-doped poly-Si layer was deposited on the top silicon to form the source and drain using a low-pressure chemical vapor deposition (LPCVD) system. A top gate oxide layer was formed by growing the 28 nm-thick SiO_2 using the thermal oxidation process. Subsequently a rapid thermal annealing (RTA) process was conducted at 850 °C for 30 s under a N_2/O_2 gas atmosphere to improve the electrical characteristics of the transistor.

In order to form the top gate electrode, a 150 nm-thick aluminium layer was deposited using an e-beam evaporator and forming gas annealing was carried out to reduce the dangling bonds and defects at the interface region at 450 °C for 30 min under a 2% H_2/N_2 atmosphere. The active channel length and width of the fabricated transistor are 10 and 20 μm respectively, and the transistor was labelled as a non-tailored thin-film transistor (TFT) in this work.

Meanwhile, to obtain high sensitivity, the thicknesses of BOX and the top gate oxide were tailored to 750 nm and 14 nm, respectively. The term 'tailored' in this paper means 'to change and optimize the thickness of the top gate oxide and BOX to enhance the amplification factor of sensor'. The other manufacturing processes were carried out in the same manner as a non-tailored TFT. The structural difference between a tailored and a non-tailored ISFET is shown in Fig. 1a.

2.1.2. Fabrication of an EG sensing device (sensing part). A p-type Si (100) wafer with a 300 nm-thick thermal SiO_2 was used as a substrate. To transmit the changes in surface potential on the sensing membrane to the top gate electrode of the TFTs, 150 nm-thick aluminium was deposited on the SiO_2 using an e-beam evaporator to serve as the contact electrode. A 50 nm-thick tin dioxide (SnO_2) film sensing membrane was formed on the aluminium electrode using the RF magnetron sputter. The RF power, the chamber pressure, and the Ar gas flow rate were maintained at 50 W, 3 mTorr, and 20 sccm, respectively. To add the chemical solution (or the buffer

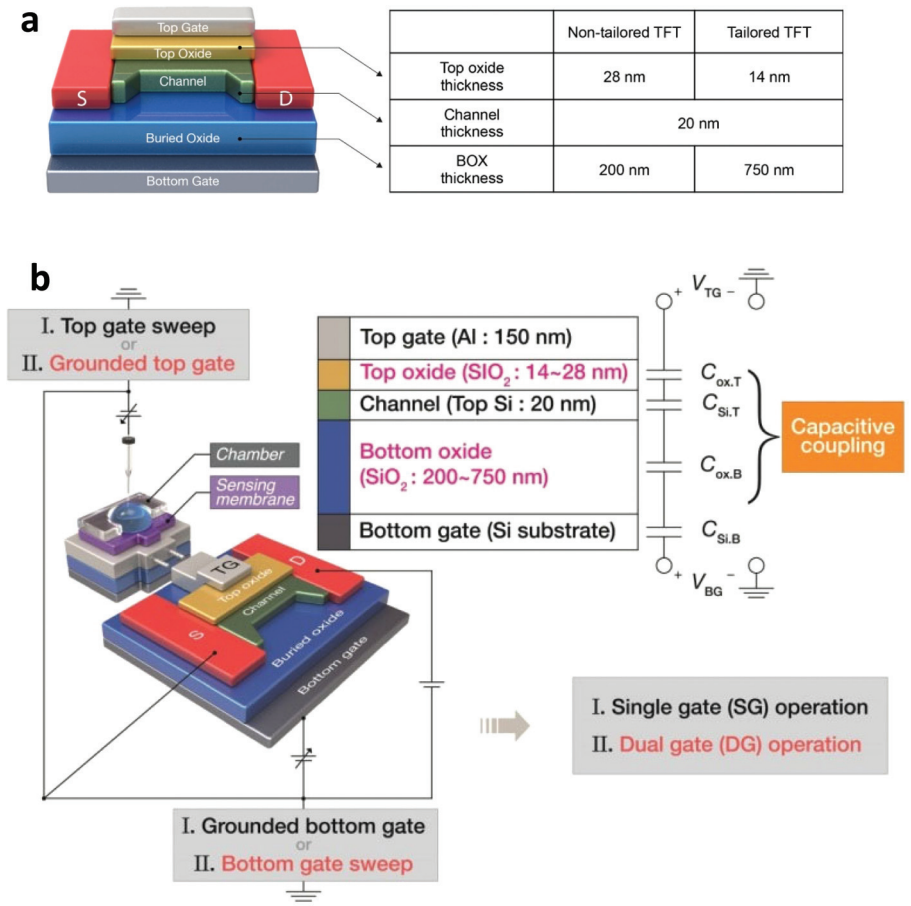

Fig. 1 (a) Structural difference between non-tailored and tailored ISFET. (b) A schematic representation of the ISFET with an EG sensing device and a description of SG and DG operation modes.

solution), a chemical chamber (polydimethylsiloxane, PDMS) was attached to the sensing membrane using silicone glue. The surface area of the sensing part was 0.5 cm^2 (internal diameter of the chamber: 0.8 cm). The surface area was adopted under the consideration that the sensor will receive sample volumes similar to the standards in clinical settings. A schematic representation of the ISFET with the EG sensing device is shown in Fig. 1b.

2.2. Sensing mechanism of the ISFET under dual-gate operation

For the DG operation, the ISFET was designed and fabricated as described in the Experimental section. As shown in Fig. 1b, the operation mode of the fabricated ISFET can be selectively driven by the switching gate biasing method. In the case of SG operations, ionic interactions at the interface between the sensing membrane and the chemical solution cause a change in the surface potential ($\Delta\psi_0$). This change is detected as a shift of the threshold voltage (ΔV_{th}^{T}) in the top gate transistor ($\Delta V_{th}^{T} = -\Delta\psi_0$). This means that the sensitivity of the SG ISFET is only determined by a change in the surface potential of the sensing membrane.[23]

On the other hand, in the case of DG operations, the sensitivity is influenced by both the bias on the bottom gate and the surface potential.[24] This is due to the capacitive coupling phenomenon originating from the unique capacitor structure between the top gate oxide and the bottom gate oxide.[25] To be specific, a shift of the threshold voltage in the bottom gate transistor (ΔV_{th}^{B}) by a $\Delta\psi_0$ of the sensing membrane can be addressed by the following simplified classic equation (1):

$$\Delta V_{th}^{B} = -\frac{C_{top}}{C_{bottom}}\Delta\psi_0 \quad (1)$$

where C_{top} and C_{bottom} are the top and bottom gate capacitances per unit area, respectively.[27] Furthermore, by replacing the capacitance values in (1) with each physical thickness, a more simplified equation can be obtained as follows:

$$\Delta V_{th}^{B} = -\frac{3t_{BOX}^{B}}{3t_{ox}^{T} + t_{Si}^{T}}\Delta\psi_0 = \frac{3t_{BOX}^{B}}{3t_{ox}^{T} + t_{Si}^{T}}\Delta V_{th}^{T} \quad (2)$$

where t_{BOX}^{B}, t_{ox}^{T}, and t_{Si}^{T} are the thicknesses of the bottom gate oxide, the top gate oxide, and the top silicon, respectively.[28] Therefore, the capacitive coupling ratio ($3t_{BOX}^{B}/3t_{ox}^{T} + t_{Si}^{T}$) is

largely affected by the physical thickness factors such as t_{BOX}^{B}, t_{ox}^{T}, and t_{Si}^{T}.

In this work, we precisely tailored the t_{BOX}^{B} and t_{ox}^{T} to enhance the sensitivity of the DG ISFET, and fixed the t_{Si}^{T} at 20 nm, the optimized thickness for the sensing performance of the DG ISFET (ESI Fig. S1†).

2.3. Measurement of ISFETs

Current *versus* voltage (*I*–*V*) measurements for the pH sensing test and the HBsAg detection were conducted using a commercial Al/AgCl reference electrode and a Hewlett-Packard 4156B high precision semiconductor parameter analyzer in a dark box to avoid light and noise interference. The sensing characteristics of the SG ISFET were measured by biasing the top reference electrode with a grounded bottom gate. In contrast, the sensing characteristics of the DG ISFET were investigated by scanning the voltage on the bottom gate with a grounded top reference electrode. A description of the SG and DG operation modes is shown in Fig. 1.

2.4. Measurement protocol for the detection of HBsAg

The measurement protocol can be described as: (1) inject a PBS buffer solution that contains a HBsAg concentration of 22.5 fg mL^{-1} (1.5 fM) onto the anti-HBsAg-immobilized sensing membrane and proceed with the reaction for 30 min; (2) wash out the previous media; (3) inject a highly controlled PBS buffer solution and measure the transfer curve; (4) pull out the PBS buffer solution; (5) repeat the same procedure by injecting a PBS buffer solution containing the HBsAg in the order of increasing concentration from 22.5 fg mL^{-1} to 22.5 ng mL^{-1} (1.5 fM–1.5 nM). In this experiment, a bovine serum albumin (BSA) solution was used to dilute the HBsAg.

3. Results and discussion

3.1. Electrical performance of the transistor

To evaluate the functionality of the transistors as transducers of the ISFET and to confirm whether or not their nanostructures were well tailored, we preliminarily measured their electrical performances. Fig. 2 shows the typical transfer curves (I_D–V_G) and the output characteristic curves (I_D–V_D) of tailored TFT (t_{ox}: 14 nm, BOX: 750 nm) and non-tailored TFT (t_{ox}: 28 nm, BOX: 200 nm) according to the gate sweep modes. Their respective electrical parameters are summarized in Table 1.

In the top gate (TG) sweep mode (Fig. 2a), both the tailored TFT and the non-tailored TFT exhibit superior electrical characteristics including a low threshold voltage (V_{th}), a good subthreshold swing (SS), and an excellent on/off current ratio. Compared with the non-tailored TFT, the tailored TFT shows a lower SS and a higher on/off current ratio. This is because the electric field in the tailored TFT was somewhat strengthened as the t_{ox} was reduced from 28 nm to 14 nm.[33] Meanwhile, in the case of the bottom gate (BG) sweep mode (Fig. 2b), the output current of the tailored TFT is much lower than that of non-tailored TFT. This result, like the result shown in Fig. 2a, is caused by different BOX thicknesses in each TFT. Ultimately, we confirmed that both t_{ox} and BOX of the tailored TFT were well adjusted and that all TFTs can faithfully perform the role of a transducer.

3.2. pH sensing test

We investigated the pH response characteristics of the ISFETs under SG and DG operations, respectively. Fig. 3a and b show the I_D–V_G curves of the SG and DG ISFETs with the non-tailored TFT (hereafter, non-tailored SG and DG ISFETs) as a transducer measured in various pH solutions (pH 3 to pH 10). As can be seen in Fig. 3a, the pH-sensitivity of the non-tailored SG ISFET was 58.88 mV per pH. Considering that the normal value of the Nernst limit is 59.6 mV per pH, the obtained sensitivity can be considered to be the maximum attainable pH-sensitivity in an ideal SG ISFET at room temperature (300 K).[26,34]

On the other hand, the non-tailored DG ISFET showed a high pH-sensitivity of 381.14 mV per pH that prominently

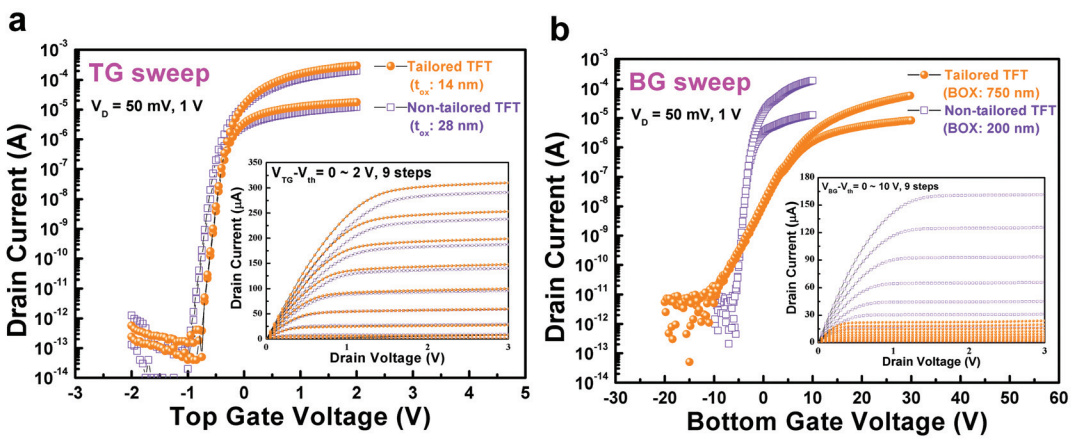

Fig. 2 Transfer curves of tailored TFT and non-tailored TFT in (a) top gate sweep mode and (b) bottom gate sweep mode, respectively. (Inset) The output characteristic curves of tailored TFT and non-tailored TFT swept by (a) TG and (b) BG, respectively.

Table 1 Electrical characteristics of the TFTs according to V_G sweep modes

Sweep mode	Transistor	V_{th} [V]	SS [mV per dec]	Maximum on/off current ratio
Top gate	Tailored TFT	−0.28	62	5.88×10^9
	Non-tailored TFT	−0.34	68	4.50×10^9
Bottom gate	Tailored TFT	−6.92	2278	6.18×10^7
	Non-tailored TFT	−2.48	485	7.01×10^8

exceeds the Nernst limit (Fig. 3b). The pH-sensitivity of the ISFET under the DG operation was increased approximately 6 times more than that of the ISFET under the SG operation.[24] Nevertheless, in order to utilize the DG ISFET as an immunosensor that detects trace amounts of analytes in undiluted media, the sensing ability needs to be enhanced.

Fig. 3c shows the I_D–V_G curves of the DG ISFET with a tailored TFT (hereafter, immuno-DG ISFET) for different pH solutions. The immuno-DG ISFET exhibited a much higher pH-sensitivity (2085.53 mV per pH) than that of the non-tailored DG ISFET. The pH response characteristics of the non-tailored and tailored ISFETs, according to their respective operation modes, are shown in Fig. 3d and summarized in Table 2 (the I_D–V_G curve of the tailored SG ISFET for different pH buffer solutions is shown in ESI Fig. S2†). As shown in Fig. 3d, in the case of the SG operation mode, the sensitivity of a tailored SG ISFET was almost identical with that of a non-tailored SG ISFET. As mentioned earlier, this is because the sensitivity of a SG ISFET can only be determined by the surface potential of the sensing membrane exposed to a pH solution.[23]

In this experiment, the pH-sensitivity of SG ISFET always showed similar values regardless of whether the TFTs were tailored or not because we used the same sensing membrane (SnO_2) in all ISFETs. Meanwhile, in the case of the DG operation mode, the pH response characteristics of a non-tailored DG ISFET and a tailored DG ISFET were significantly different although there was the same change in surface potential by pH variation. The experimental coupling ratio ($\Delta V_{th}^B/\Delta V_{th}^T$) of a non-tailored DG ISFET attained from the pH sensing test was ~6.47, whereas a tailored DG ISFET showed ~35.77.

The error percentage between the experimental coupling ratio and the theoretical coupling ratio ($3t_{BOX}^B/3t_{ox}^T + t_{Si}^T$) was 10.81% in a non-tailored ISFET and 1.45% in a tailored ISFET, respectively. This means that we can maximize and optimize the sensitivity of the ISFET sensors by precisely tuning the

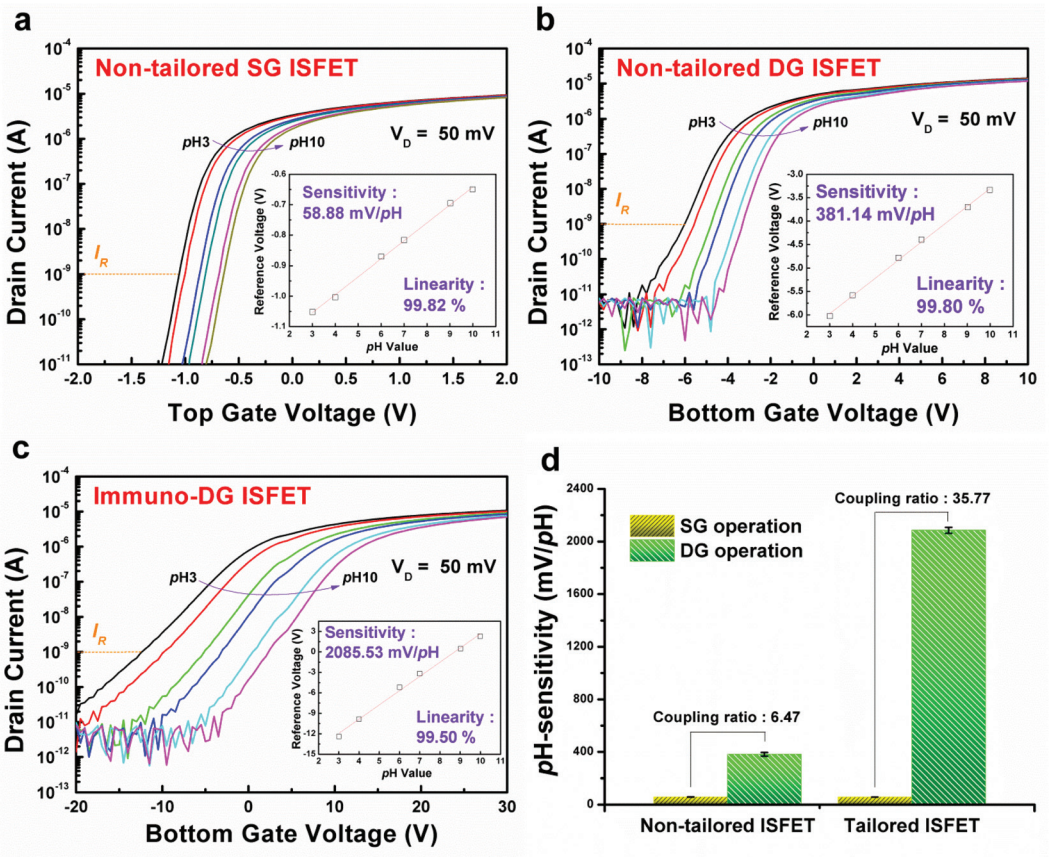

Fig. 3 I_D–V_G curves of the non-tailored (a) SG ISFET, (b) DG ISFET, and (c) immuno-DG ISFET for various pH buffer solutions. The drain bias is set at 50 mV. The response voltage (V_R) for each pH buffer solution (pH 3 to pH 10), shown in the insets, was defined as the corresponding gate voltage to the drain current (reference current: I_R) of 1 nA. (d) The pH-sensitivity of the standard and tailored ISFETs with SG and DG operation modes.

Table 2 Sensing properties of the non-tailored ISFET and the tailored ISFET according to the operation modes

Sensor	Operation mode	Sensitivity [mV per pH]	Linearity [%]	$\Delta V_{th}^{B}/\Delta V_{th}^{T}$ ratio	Coupling ratio error percentage [%]
Non-tailored ISFET	SG	58.88	99.82	6.47	10.81
	DG	381.14	99.80		
Tailored ISFET	SG	58.29	99.68	35.77	1.45
	DG	2085.53	99.50		

device design; the enhancement of sensitivity by DG operation does not mean a simple improvement of the signal-to-noise ratio. In our previous work, by evaluating the instability factors of a DG ISFET for long-term usage, we confirmed that reliability and stability in a DG ISFET were much more improved than that in a SG ISFET.[35,36] Consequently, this approach is very important for biosensing applications because enhancements of sensitivity and reliability can provide great potential improvement in monitoring the small signals that arise from biological events in the system.

3.3. Detection of HBsAgs

In order to verify the feasibility of using our sensor in a biological environment, we used the immuno-DG ISFET as a biosensor for detecting HBsAgs that range from 22.5 fg mL^{-1} to 22.5 ng mL^{-1} (1.5 fM–1.5 nM). Fig. 4a represents the V_{th} shift according to HBsAg concentration in a HBsAg-Ab reaction. The I_D–V_G curves were measured in a 0.001× PBS environment after washing out the HBsAgs (a detailed measurement protocol for the detection of HBsAg is described in the Experimental section). As the HBsAg concentration increased, the V_{th} was shifted in the negative direction. The negative shift of V_{th} results from the change in surface potential by the HBsAg-Ab reaction.[37] Because the HBsAgs bear strong negative surface charges (zeta potential: −35.7 mV), the positive ions in the media cluster near the HBsAgs[32] (zeta potential distributions for HBsAgs and anti-HBsAgs are shown in ESI Fig. S3†). These additional positive charges make the surface potential of the sensing membrane more positive and help the channel resistance to decrease.[38] Thus, a negative shift in V_{th} is observed.

As the control experiment, HBsAgs were injected on the surface where anti-HBsAgs were not immobilized, as shown in Fig. 4b, and we could not observe the V_{th} shift like that of the HBsAg-Ab reaction. These results mean that our immuno-DG ISFET has outstanding sensitivity and specificity for detecting the HBsAgs in a dynamic detection range of 10^6 from 22.5 fg mL^{-1} to 22.5 ng mL^{-1} (I_D–V_G curves of the non-tailored SG and DG ISFETs according to HBsAg concentration in the HBsAg-Ab reaction are shown in ESI Fig. S4†).

3.4. Sensing performance analysis

Fig. 5a shows the reference voltage shift (ΔV_R) according to the ionic strength of the PBS buffer solution in HBsAg-Ab detection using the immuno-DG ISFET. An interesting phenomenon

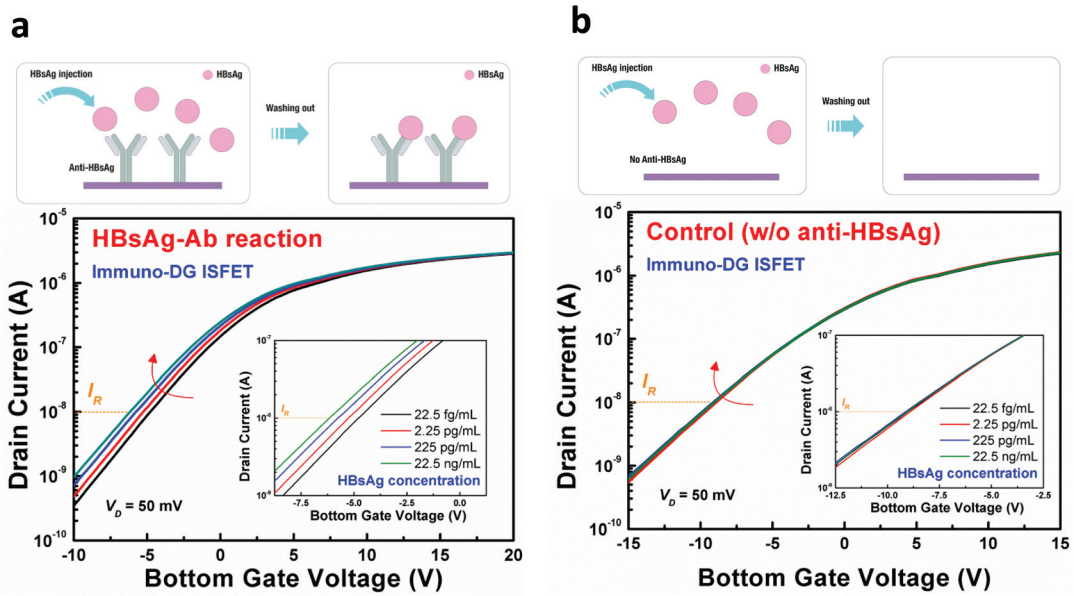

Fig. 4 I_D–V_G curves of the immuno-DG ISFET according to HBsAg concentration in (a) HBsAg-Ab reaction and (b) control experiment (no-antibody reaction).

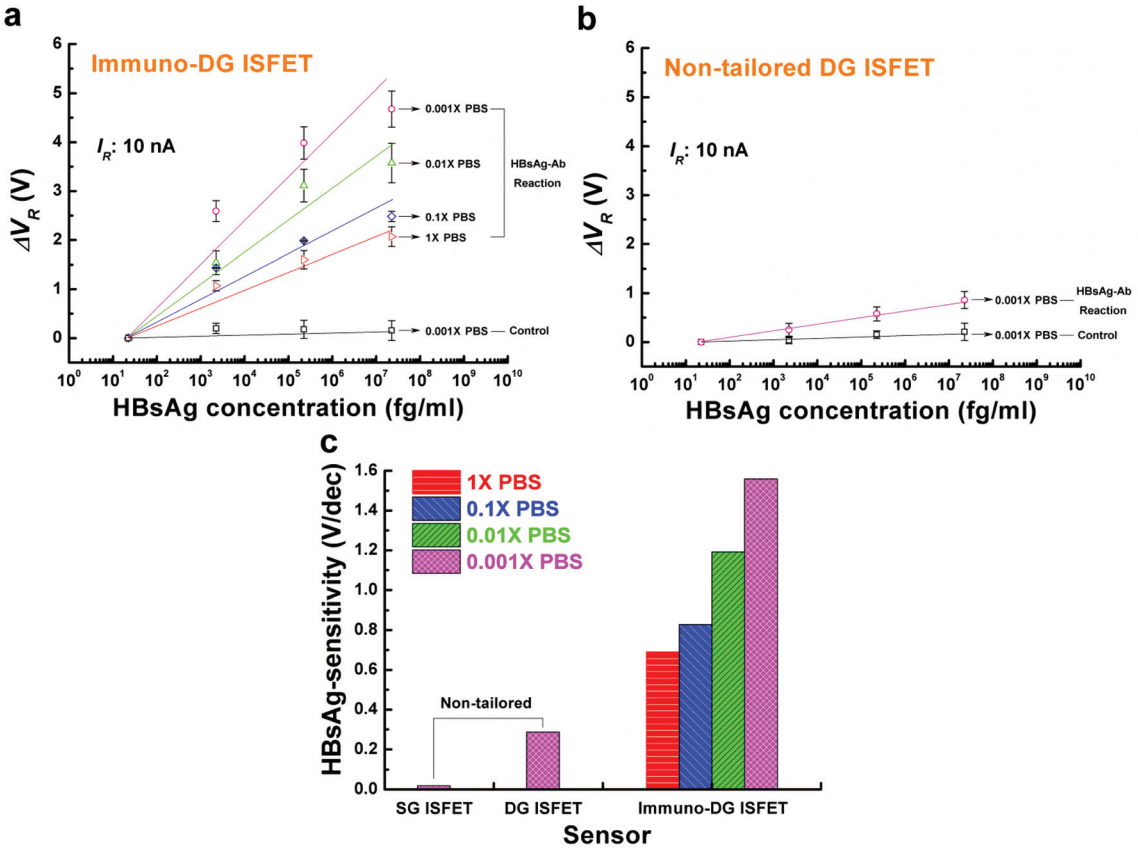

Fig. 5 Variations of V_R (ΔV_R) according to different HBsAg concentrations in (a) immuno-DG ISFET and (b) non-tailored DG ISFET, respectively. The V_R was the corresponding gate voltage to the drain current of 10 nA under the drain voltage of 50 mV. (c) HBsAg-sensitivity depending on ionic strength of PBS in tailored DG ISFET and comparison with HBs-sensitivities in other sensors.

seen in the result is the large ΔV_R in the low ionic strength of PBS buffer solution (0.001× PBS). This is related to the Debye screening length (λ_D), which in turn depends on the ionic strength of PBS buffer solution. Because the λ_D increases as the ionic strength of PBS decreases, more HBsAg-Ab reactions can be detected in a PBS solution with low ionic strength.[22,30] Consequently, as shown in Fig. 5a, the ΔV_R was the largest in 0.001× PBS. Fig. 5b shows the ΔV_R measured in a 0.001× PBS environment using the non-tailored DG ISFET.

Compared with the immuno-DG ISFET, the non-tailored DG ISFET exhibited a much lower ΔV_R in the same 0.001× PBS environment. This is due to the low coupling ratio of the non-tailored DG ISFET that was shown in the pH sensing test. Fig. 5c shows the average detection sensitivity for HBsAg-Ab reactions in each sensor. Compared with the HBsAg-sensitivity (18.67 mV, 0.001× PBS) of the non-tailored SG ISFET, the non-tailored DG ISFET showed a much higher sensitivity (287.1 mV, 0.001× PBS). Furthermore, the HBsAg-sensitivity (1558.9 mV, 0.001× PBS) of the immuno-DG ISFET was more significantly enhanced than that of the non-tailored DG ISFET. Here, it is noteworthy that the HBsAg-sensitivity of the SG ISFET is excessively low compared to those of the non-tailored and tailored DG ISFETs. This is because the sensing ability of the SG ISFET is not enough to accurately detect the small changes in surface potential that arise from the HBsAg-Ab reactions.[25,27]

This result indicates that the DG ISFETs can enhance not only the sensing signal, but also the detection limit of the target molecule concentration. Consequently, by using the immuno-DG ISFET, we successively detected trace amounts of HBsAg in undiluted 1× PBS with a high sensitivity of ~690.15 mV. This sensitivity is much higher than that of the non-tailored DG ISFET (~287.1 mV) measured in 0.001× PBS.

4. Conclusions

In this study, for the first time, a highly sensitive immuno-DG ISFET biosensor was proposed to detect trace amounts of HBsAg in undiluted 1× PBS solution. Compared to the non-tailored DG ISFET as well as SG ISFET, the proposed immuno-DG ISFET exhibited a significantly increased sensitivity and an improved limit of detection (LOD). Furthermore, the immunosensor even had a lower LOD value compared to those of other conventional methods (Table 3). In conclusion, through these enhancements, we have successfully resolved the stubborn pro-

Table 3 Detection limit comparison, conducted by CNT, graphene, and nanowire, between our proposed immunosensor and other FET-based immunosensors

Technique	Immunosensor	Analyte	Detection limit	Ref.
CNT	Single-walled CNT FET	Prostate-specific antigen	7 pM	13
Graphene	Aptamer-modified graphene FET	Immunoglobulin E protein	47 nM	17
Nanowire	SiNW FET	Prostate-specific antigen	0.15 pM	21
Our sensor	Tailored-DG FET	Hepatitis B surface antigen	1.5 fM	This work

blems of current transistor-based immunosensors for practical applications: low sensitivity by the short λ_D in media with high ion concentration and the time-consuming media preconditioning issue. All the results reported in this paper strongly support that the proposed immuno-DG ISFET sensor has great potential for biomedical device applications.

Acknowledgements

This work was supported by the KIST (ORP #2E25722, AMC-KIST TRC #2E25502, Institutional Project #2E25260, and CTP #2V03990). The authors appreciate Mr Suchang Mun for help with graphical artworks.

References

1 J. L. Dienstag, *N. Engl. J. Med.*, 2008, **359**, 1486–1500.
2 X. Zhang, Q. Zhang, Q. Peng, J. Zhou, L. Liao, X. Sun, L. Zhang and T. Gong, *Biomaterials*, 2014, **35**, 6130–6141.
3 A. Jemal, F. Bray, M. M. Center, J. Ferlay, E. Ward and D. Forman, *Ca-Cancer J. Clin.*, 2011, **61**, 69–90.
4 C. L. Lin and J. H. Kao, *J. Gastroenterol. Hepatol*, 2011, **26** (Suppl 1), 123–130.
5 X. Li, H. Feng, W. N. Chen and V. Chan, *Biomaterials*, 2010, **31**, 1894–1903.
6 L. European Association For The Study Of The, *J. Hepatol.*, 2012, **57**, 167–185.
7 W. F. Carman, L. Wallace, J. Korula, R. MacPhee, L. Mimms and R. Decker, *Lancet*, 1995, **345**, 1406–1407.
8 C. A. Schable and J. E. Maynard, *J. Clin. Microbiol.*, 1982, **16**, 973–975.
9 A. Tarasov, M. Wipf, R. L. Stoop, K. Bedner, W. Fu, V. A. Guzenko, O. Knopfmacher, M. Calame and C. Schönenberger, *ACS Nano*, 2012, **6**, 9291–9298.
10 J. M. Rothberg, W. Hinz, T. M. Rearick, J. Schultz, W. Mileski, M. Davey, J. H. Leamon, K. Johnson, M. J. Milgrew, M. Edwards, J. Hoon, J. F. Simons, D. Marran, J. W. Myers, J. F. Davidson, A. Branting, J. R. Nobile, B. P. Puc, D. Light, T. A. Clark, M. Huber, J. T. Branciforte, I. B. Stoner, S. E. Cawley, M. Lyons, Y. Fu, N. Homer, M. Sedova, X. Miao, B. Reed, J. Sabina, E. Feierstein, M. Schorn, M. Alanjary, E. Dimalanta, D. Dressman, R. Kasinskas, T. Sokolsky, J. A. Fidanza, E. Namsaraev, K. J. McKernan, A. Williams, G. T. Roth and J. Bustillo, *Nature*, 2011, **475**, 348–352.
11 C. Toumazou, L. M. Shepherd, S. C. Reed, G. I. Chen, A. Patel, D. M. Garner, C. J. Wang, C. P. Ou, K. Amin-Desai, P. Athanasiou, H. Bai, I. M. Brizido, B. Caldwell, D. Coomber-Alford, P. Georgiou, K. S. Jordan, J. C. Joyce, M. La Mura, D. Morley, S. Sathyavruthan, S. Temelso, R. E. Thomas and L. Zhang, *Nat. Methods*, 2013, **10**, 641–646.
12 J. Oh, G. Yoo, Y. W. Chang, H. J. Kim, J. Jose, E. Kim, J. C. Pyun and K. H. Yoo, *Biosens. Bioelectron.*, 2013, **50**, 345–350.
13 C. Li, M. Curreli, H. Lin, B. Lei, F. Ishikawa, R. Datar, R. J. Cote, M. E. Thompson and C. Zhou, *J. Am. Chem. Soc.*, 2005, **127**, 12484–12485.
14 S. Mao, G. Lu, K. Yu, Z. Bo and J. Chen, *Adv. Mater.*, 2010, **22**, 3521–3526.
15 Y. Ohno, K. Maehashi, Y. Yamashiro and K. Matsumoto, *Nano Lett.*, 2009, **9**, 3318–3322.
16 W. Fu, C. Nef, A. Tarasov, M. Wipf, R. Stoop, O. Knopfmacher, M. Weiss, M. Calame and C. Schonenberger, *Nanoscale*, 2013, **5**, 12104–12110.
17 Y. Ohno, K. Maehashi and K. Matsumoto, *J. Am. Chem. Soc.*, 2010, **132**, 18012–18013.
18 M. Wipf, R. L. Stoop, A. Tarasov, K. Bedner, W. Fu, I. A. Wright, C. J. Martin, E. C. Constable, M. Calame and C. Schönenberger, *ACS Nano*, 2013, **7**, 5978–5983.
19 Y. D. Ivanov, T. O. Pleshakova, A. F. Kozlov, K. A. Malsagova, N. V. Krohin, V. V. Shumyantseva, I. D. Shumov, V. P. Popov, O. V. Naumova, B. I. Fomin, D. A. Nasimov, A. L. Aseev and A. I. Archakov, *Lab Chip*, 2012, **12**, 5104–5111.
20 I. N. Kholmanov, M. D. Stoller, J. Edgeworth, W. H. Lee, H. Li, J. Lee, C. Barnhart, J. R. Potts, R. Piner and D. Akinwande, *ACS Nano*, 2012, **6**, 5157–5163.
21 G. Zheng, X. P. Gao and C. M. Lieber, *Nano Lett.*, 2010, **10**, 3179–3183.
22 M. S. Makowski and A. Ivanisevic, *Small*, 2011, **7**, 1863–1875.
23 S. Chen, J. G. Bomer, E. T. Carlen and A. Van Den Berg, *Nano Lett.*, 2011, **11**, 2334–2341.
24 M. Spijkman, E. C. P. Smits, J. F. M. Cillessen, F. Biscarini, P. W. M. Blom and D. M. de Leeuw, *Appl. Phys. Lett.*, 2011, **98**, 043502.
25 M.-J. Spijkman, J. J. Brondijk, T. C. T. Geuns, E. C. P. Smits, T. Cramer, F. Zerbetto, P. Stoliar, F. Biscarini,

P. W. M. Blom and D.M. de Leeuw, *Adv. Funct. Mater.*, 2010, **20**, 898–905.
26 O. Knopfmacher, A. Tarasov, W. Fu, M. Wipf, B. Niesen, M. Calame and C. Schonenberger, *Nano Lett.*, 2010, **10**, 2268–2274.
27 M. J. Spijkman, K. Myny, E. C. Smits, P. Heremans, P. W. Blom and D. M. de Leeuw, *Adv. Mater.*, 2011, **23**, 3231–3242.
28 H. J. Jang and W. J. Cho, *Sci. Rep.*, 2014, **4**, 5284.
29 A. Matsumoto and Y. Miyahara, *Nanoscale*, 2013, **5**, 10702–10718.
30 A. Vacic, J. M. Criscione, N. K. Rajan, E. Stern, T. M. Fahmy and M. A. Reed, *J. Am. Chem. Soc.*, 2011, **133**, 13886–13889.
31 E. Stern, R. Wagner, F. J. Sigworth, R. Breaker, T. M. Fahmy and M. A. Reed, *Nano Lett.*, 2007, **7**, 3405–3409.
32 H. J. Jang, J. Ahn, M. G. Kim, Y. B. Shin, M. Jeun, W. J. Cho and K. H. Lee, *Biosens. Bioelectron.*, 2015, **64**, 318–323.
33 Y. Yamamoto, K. Kita, K. Kyuno and A. Toriumi, *Appl. Phys. Lett.*, 2006, **89**, 032903.
34 D. Sarkar, W. Liu, X. Xie, A. C. Anselmo, S. Mitragotri and K. Banerjee, *ACS Nano*, 2014, **8**, 3992–4003.
35 I. K. Lee, K. H. Lee, S. Lee and W. J. Cho, *ACS Appl. Mater. Interfaces*, 2014, **6**, 22680–22686.
36 H.-J. Jang and W.-J. Cho, *Appl. Phys. Lett.*, 2012, **100**, 073701.
37 T. Sakata, M. Ihara, I. Makino, Y. Miyahara and H. Ueda, *Anal. Chem.*, 2009, **81**, 7532–7537.
38 D. Goncalves, D. M. Prazeres, V. Chu and J. P. Conde, *Biosens. Bioelectron.*, 2008, **24**, 545–551.